

LoUQAL: Low-fidelity informed Uncertainty Quantification for Active Learning in the chemical configuration space

Vivin Vinod^{1*} and Peter Zaspel¹

¹School of Mathematics and Natural Sciences, University of Wuppertal, Germany.

*Corresponding author(s). E-mail(s): vinod@uni-wuppertal.de

Abstract

Uncertainty quantification is an important scheme in active learning techniques, including applications in predicting quantum chemical properties. In quantum chemical calculations, there exists the notion of a fidelity, a less accurate computation is accessible at a cheaper computational cost. This work proposes a novel low-fidelity informed uncertainty quantification for active learning with applications in predicting diverse quantum chemical properties such as excitation energies and *ab initio* potential energy surfaces. Computational experiments are carried out in order to assess the proposed method with results demonstrating that models trained with the novel method outperform alternatives in terms of empirical error and number of iterations required. The effect of the choice of fidelity is also studied to perform a thorough benchmark.

Keywords: active learning, potential energy surface, quantum chemistry, DFT, GPR, uncertainty quantification, excitation energies

Notation/Abbreviation	Description
ML	Machine Learning
QC	Quantum Chemistry
AL	Active Learning
UQ	Uncertainty Quantification
GPR	Gaussian Process Regression

Notation/Abbreviation	Description
MAE	Mean Absolute Error
CCSD(T)	Coupled Cluster Singles Doubles (Triples)
MP2	Møller-Plesset Perturbation
HF	Hartree-Fock
CM	Coulomb Matrix
DFT	Density Functional Theory
SMA	2-(methylinomethyl)phenol
DMABN	4-(dimethylamino) benzonitrile
o-HBDI	4-(2-hydroxybenzylidene)-1,2-dimethyl-1H-imidazol-5(4H)-one
PCA	Principle Component Analysis
f	Index of ordered fidelities
F	Target fidelity
f_b	baseline fidelity
\mathcal{T}^f	Training dataset with fidelity f
N_{train}^f	Number of training samples used at f
\mathcal{X}	Set of all inputs, \mathbf{x} , from \mathcal{T}^f
\mathbf{X}	Vector of all inputs from \mathcal{T}^f
\mathbf{Y}	Vector of all outputs from \mathcal{T}^f
\mathcal{V}	Holdout test set computed at F
\mathcal{U}	Set of all molecular configurations available for AL
\mathcal{A}	Set of molecular configurations chosen by AL
g^f	Exact function at f to be learned
\hat{g}^f	Learned function at f ; prediction of ML model at f
\bar{g}^f	Average prediction from ML-ensemble at f
ϕ_{var}	GPR variance based UQ
ϕ_{greedy}	Greedy adaptive sampling UQ
$\phi_{5\times}$	5-ensemble based UQ
$\text{LoUQ}/\phi_{\text{LoUQ}}^{f_b}$	Low-fidelity informed UQ with f_b

Main

The use of machine learning (ML) as a tool to speed up the computation of quantum chemistry (QC) properties has gained momentous pace over the recent years [1–5]. The expense of running QC calculations has now been outsourced to the process of generating training data for such ML models. Once trained, these models offer rapid *predictions* of the QC property of interest such as excitation energy, the gap between ground state and excited state energies of a molecule [6, 7]. Once a specific problem is identified for which ML models are to be used, such as predicting excitation energies, training data is generated with a specific accuracy, or *fidelity*. Depending on the amount of computational effort that is expended, fidelities can be high accuracy or low accuracy (and low cost). The fidelity of QC property that is finally used for predictions is referred to as the *target fidelity*. The process of generating training data

for a target fidelity is a fundamental step in this pipeline for which it is crucial that the right molecular configurations be selected in order to provide maximal information to the ML model.

Active learning (AL) strategies for ML have facilitated the selection of optimal training samples. There exist several heuristics in AL for the selection of training data such as low-confidence sampling [8] or highest-change sampling [9]. A common low-confidence approach is the estimation of an *uncertainty quantification* (UQ) which is an indicator of how much variance a trained model has due to the specific choice of training data. In ML approaches such as Gaussian Process Regression (GPR), the variance of the predictor is a quantity that is used as a metric for UQ [10] and is obtained during the training of the model. Some works have extended this notion to training several GPR models on subsets of training data and use the predictive variance of the *ensemble* as the UQ for AL [11–15]. In another approach, two distinct ML models, characterized by different architectures, are trained and the samples which indicate the highest difference in predictions with these models are added to the training dataset [16]. Another UQ measure, referred to as greedy adaptive selection scheme (ϕ_{greedy}), is an idealized way to select training samples [17, 18]. The method first computed the empirical error for each data sample of interest. The data point with the highest error is then added to the training dataset. The ϕ_{greedy} renders the ML-QC pipeline redundant since it requires explicit knowledge of the reference QC property for each molecular configuration in order to compute the UQ measure. Thus, the best UQ measure, ϕ_{greedy} , is only used as a comparison for the efficacy of other UQ measures [19]. Any UQ measure that performs similarly to ϕ_{greedy} in terms of resulting empirical error would be a good UQ measure for AL.

A useful tool in order to evaluate ML models resulting from UQ-based AL is *calibration* which refers to the trend observed between computed UQ measure and empirical error [20, 21]. A well calibrated ML model is identified if lower uncertainty corresponds to lower errors, ensuring that the ML model’s notion of uncertainty does in fact translate into its effect on empirical error. A recent study in the use of difference UQ for AL in QC identified that the use of common UQ measures such as ϕ_{var} and $\phi_{n\times}$ results in an ML model performing worse than one built with either ϕ_{greedy} or random sampling of the configuration space for training samples [19]. The aforementioned UQs only identified training samples with high bias, overemphasizing the boundaries of the configuration space. The resulting ML models for ML interatomic potentials were found to have poor calibration. A possible strategy to improve model calibration was presented in ref. [22] with the use of isotonic regression as a *posthoc* measure showing improvement in the empirical error of the resulting ML model for prediction of both energy and forces.

Motivated by the lack of a UQ measure that is well calibrated, in this work, a novel Low-fidelity informed Uncertainty Quantification measure (LoUQ) is developed and benchmarked. Indicated hereon as ϕ_{LoUQ} , this approach uses the QC property computed as a cheaper fidelity to train an *ad hoc* GPR model. Using this model, the absolute difference in prediction and reference is used as the uncertainty to select the molecular configuration for each iteration of the AL scheme. Benchmark experiments in the following section establish this method as superior to not only existing UQs but

also to the random sampling of molecular configuration space. Numerical experiments show that the LoUQAL models perform as well as the ones built with the best UQ measure of ϕ_{greedy} . Evidence to this end is shown for three distinct QC properties with the LoUQAL approach outperforming all common UQ measures in each case.

Results

The workflow utilized to perform the computational benchmarks in this work is shown in Fig. 1. Three distinct QC properties are chosen from three datasets in order to thoroughly benchmark the LoUQAL method. In each case, the available data is first partitioned into a 90/10 split of training pool and holdout test set data. The latter is used to compute the empirical error at the target fidelity, reported as MAE. From the training pool, an initial set of 100 random molecular configurations is chosen for which the QC properties are acquired to build the training dataset at the target fidelity F . Hyper-parameters for the GPR model are optimized using marginal log-likelihood (see section S1.5) over this initial dataset and a GPR model is trained and used to compute different UQ measures for the remaining molecular configurations in the AL data pool (\mathcal{U}). The configuration with the highest value of the UQ measure is selected and the QC property is computed for this point at the target fidelity to be added to the training dataset. This process is repeated each iteration of the AL scheme for a total of 2000 iterations. At each iteration, the MAE is computed and finally reported as a learning curve to study the error trend as a function of number of training samples. In the experiments, ϕ_{greedy} , ϕ_{var} , $\phi_{5\times}$ (5-ensemble approach), and the novel ϕ_{LoUQ} are compared against the random sampling approach (see [Uncertainty Quantification for Active Learning](#) for details). While the common UQs use some knowledge about the molecular configuration space, ϕ_{LoUQ} has the additional information of the QC property landscape at a cheaper fidelity as indicated in the lower left corner of Fig. 1. This is in contrast to the case for ϕ_{greedy} where the QC property landscape is known for the target fidelity itself.

The experiments carried out are broadly categorized into two parts: first, to evaluate LoUQAL for the case where the notion of fidelity is established across QC methods and second where fidelities are defined by the choice of a basis set across a single QC method. Both these benchmarks allow for a controlled yet robust analysis of the proposed method against existing UQ based AL schemes. The first case for cross-QC-method testing is performed for the prediction of atomization energies of the QM7b dataset for a collection of several molecules [23], and *ab initio* potential energy surfaces (PES) of two molecules from the VIB5 dataset [24]. The second case of cross-basis testing is performed for the more challenging QC property of excitation energies taken from the QeMFi dataset [25] for nine different molecules.

Cross-QC-Method LoUQAL

QC methods offer a clear hierarchy in terms of computational cost and achieved accuracy of calculation. It is relevant, therefore, to test LoUQAL for such a definition of ordered hierarchy of fidelities. In the following experiments, cross-QC-method testing

of LoUQAL is performed with empirical error being assessed as a function of training set size - reported as learning curves.

Predicting Atomization Energies

The QM7b dataset [23] consists of atomization energies of a total of 7211 molecules computed with 3 different QC methods CCSD(T), MP2, HF. For each, three basis sets are used, STO3G, 631G, and ccpVDZ (see section S1.3.1). To test cross-QC capabilities of LoUQAL, a basis set is fixed and the CCSD(T) target fidelity is chosen. MP2 and HF are then used as the baseline fidelities. The SLATM descriptor [26] is used as a representation of the molecules in order to retain permutational invariance [27] (see section S1.4).

Resulting learning curves are shown in Fig. 2. In all three panes, the x-axis reports number of training samples, each chosen during a specific run of the AL iteration, while the y-axis reports MAE on the holdout test set. Consider the case for basis set ccpVDZ. The learning curve corresponding to $\phi_{5\times}$ performs the worst in this case with a higher error throughout all training set sizes. Next comes the one for ϕ_{var} with an error above the 5 kcal/mol mark for $N_{\text{train}}^{\text{CCSD(T)}-\text{ccpVDZ}} = 2,100$. Both these AL schemes perform worse than randomly sampling training data across the configuration space. This indicates that these UQs do not result in a meaningful reduction of empirical error. On the other hand, the $\phi_{\text{greedy-AL}}$ approach results in a learning curve that is steeper and results in a much lower error as expected since this approach has full knowledge of the target fidelity atomization energy landscape. The novel LoUQAL method, indicated as $\phi_{\text{LoUQ}}^{(f_b)}$ with f_b as HF or MP2, performs nearly identical to the $\phi_{\text{greedy-AL}}$ method with a similar slope resulting in an MAE of about 3 kcal/mol for $N_{\text{train}}^{\text{CCSD(T)}-\text{ccpVDZ}} = 2,100$. Identical observations can be made for the other two basis sets where the LoUQAL method outperforms random sampling and the common UQ based AL schemes.

One inference from these learning curves can be readily made about LoUQAL vis-à-vis other UQs based AL. The x-axis represents N_{train} which is direct measure also of the number of iterations of the AL scheme. For a fixed number of AL iterations, the LoUQAL outperforms all other models in terms of empirical error. Alternatively, if one had a threshold of error that was desired, say 5 kcal/mol, then the LoUQAL method achieves this error for a fewer number of AL iterations (~ 700) than the random sampling approach ($\sim 2,000$) while the $\phi_{\text{var-AL}}$ and $\phi_{5\times}$ will likely reach this error with a few more iterations than 2,000.

A comprehensive test of defining fidelities as a combination of QC method *and* basis set choice is performed in the supplementary information section S2.1 resulting in learning curves shown in Fig. SF1. In this case as well, the LoUQAL method outperforms the random sampling of configuration space while being close to the accuracy offered by the $\phi_{\text{greedy-AL}}$ scheme. With the target fidelity being set to CCSD(T)-ccpVDZ, one notices that the choice of the basis set makes more of a difference than the choice of the QC method. The $\phi_{\text{LoUQ}}^{(\text{CCSD(T)}-\text{STO3G})}$ -AL performs worse than the $\phi_{\text{LoUQ}}^{(\text{HF-ccpVDZ})}$ -AL scheme in terms of empirical error.

Predicting *ab initio* Potential Energy Surfaces

The VIB5 database contains the CH_3Cl and CH_3F molecules with the ground state *ab initio* PES computed with varying methods, the most expensive being CCSD(T) with the ccpVQZ basis set [24]. In order to perform a reasonable assessment of the AL strategies, for each molecule 15,000 samples were randomly chosen and the procedure described before was carried out to separate them into training pool and test set. Since the experiments were carried out for the same molecule and no cross molecule tests were carried out, the unsorted CM matrix representation [28] was used (see section S1.4). This simple representation does not violate any permutation invariance since the atoms are numbered identically across the entire dataset of each molecule in VIB5. The cheaper fidelities used as f_b are a composite of change in QC method and basis set, namely MP2-ccpVTZ, HF-ccpVQZ, HF-ccpVTZ (in decreasing accuracy compared to the target fidelity).

The resulting learning curves that assess different UQ-AL strategies are shown in Fig. 3 for both molecules. Consider the case for CH_3Cl on the left-hand side of the figure. The y-axis presents the MAE of the GPR model built with a certain number of training samples which are represented on the x-axis. Both axes are logarithmically scaled. The ϕ_{var} -AL scheme performs poorest showing a gradual slope of the learning curve. A similar observation is made for the $\phi_{5\times}$ -AL with both resulting models showing an MAE around 8 kcal/mol for $N_{\text{train}}^{\text{CCSD(T)}-\text{ccpVQZ}} = 2, 100$. The random sampling approach results in a steeper slope than using either of these UQ-AL schemes indicating that both these UQ measures lack performance. On the other hand, the $\phi_{\text{LoUQ}}^{f_b}$ -AL scheme performs better than the random sampling approach and results in an MAE as good as the ϕ_{greedy} -AL approach. The $\phi_{\text{LoUQ}}^{f_b}$ -AL built with all three f_b perform similar to each other with no apparent difference in the overall empirical error arising from the final models. However, it is to be noted that the random sampling approach does perform similar in MAE to the LoUQAL method. This can be explained by noting that the two molecules used in this experiment are rather small and it could be relatively easier for ML models to learn the *ab initio* PES for such small molecules even by choosing random training samples. Regardless, the negative slope of the learning curves for both random sampling and LoUQAL indicate that further addition of training samples could further reduce the error of the trained GPR model. Thus, LoUQAL is seen to outperform the standard UQ measures in the case of PES reconstruction.

Cross-Basis LoUQAL for Excitation Energies

The second set of computational benchmarks that are set for the LoUQAL method is the prediction of excitation energies with fidelities being defined as the choice of basis set while fixing the QC method to be DFT. Already in Fig. SF1 it was observed that the choice of the basis set made a stronger difference than the choice of the QC method while predicting the atomization energies. Therefore, it is relevant to check whether this effect is visible in the case of a more complex QC property, the excitation energy.

The QeMFi dataset contains 9 molecules, 15,000 configurations each, with several excitation energies computed with the DFT formalism using varying basis set sizes [25, 29]. The target fidelity is therefore def2-TZVP (hereon denoted as TZVP) with

f_b being cheaper basis sets def2-SVP (denoted hereon as SVP), 631G, and 321G. The benchmarks are carried out for each individual molecule and therefore the unsorted CM [28] are used.

Learning curves for the prediction of excitation energies of each molecule in QeMFi are shown in Fig. 4 once again depicting the different UQ measures studied in this work alongside the random sampling approach. The axes are scaled logarithmically with each subplot showing different ranges of the y-axis for better visibility. For each of the nine molecules identical observations can be made. The ϕ_{var} and $\phi_{5\times}$ based AL perform worse than the random sampling of configuration space. On the other hand, the LoUQAL scheme results in a GPR model that provides much steeper slopes, almost same as the ϕ_{greedy} -AL approach. This once again indicates that the novel LoUQ results in a trained ML model that reduces the empirical error of prediction performing better than the random sampling approach and common UQ measures. It becomes clear that LoUQAL achieves lower error at a lower number of AL iterations in comparison to the other UQ-AL approaches.

Visualizing Uncertainty Quantification

Having benchmarked the LoUQAL method for different QC properties, it is useful to also establish its credibility in a visual comparison to the ϕ_{greedy} -AL scheme. The learning curves from the previous sections already provide numerical evidence of the performance of the LoUQAL scheme. Since the ML-QC pipeline converts molecular configurations to representations/descriptors, it is relevant to look at this as a proxy space. To this end, the molecular descriptors are passed through a principle component analysis (PCA) with the two leading components being used to visualize the proxy space.

Fig. 5 shows the 2D PCA for CH_3Cl from VIB5, DMABN, thymine, and o-HBDI from QeMFi. The total AL pool is shown in the foreground. For each molecule, three specific scatter points are highlighted in order to compare ϕ_{greedy} and $\phi_{\text{LoUQ}}^{f_b}$. The first set is the collection of points that are selected during the first 500 AL iteration by both UQ measures. The second is those selected by the ϕ_{greedy} measure and third is that selected by the $\phi_{\text{LoUQ}}^{f_b}$ method introduced in this work. For CH_3Cl , f_b is HF-ccpVTZ while for the molecules of QeMFi it is the 321G fidelity. In all 4 molecules it can be seen that ϕ_{LoUQ} selects nearly all the same points as the ϕ_{greedy} UQ measure. In contrast, Fig. SF2 in the supplementary information compares the points selected by ϕ_{var} and ϕ_{LoUQ} with significantly different points being selected by both these UQ measures (see section S2.2 for more details). This is an indicator that the herein developed method performs as well as the greed adaptive scheme identifying the right areas of high uncertainty in the proxy molecular configuration space.

Calibration Curves

For the same four molecules as before, Fig. 6 reports the calibration curves, a plot of empirical error against the chosen UQ measure. The x-axis reports the MAE in kcal/mol, the left y-axis notes the normalized ϕ_{LoUQ} , and the right y-axis reports the normalized ϕ_{var} . It can be observed that for all four molecules, the empirical error

decreases with a decrease in ϕ_{LoUQ} for each step of the AL iteration (indicated by the color of the markers). This decrease is steady and without any discontinuities meaning that LoUQ was able to identify the right data point with highest uncertainty in order to translate that into a lower empirical error in the trained GPR model. On the other hand the ϕ_{var} UQ measure results in cases with discontinuities (CH_3Cl and o-HBDI), constant empirical errors for decreasing uncertainty (DMABN), and in the case of thymine an increase in empirical error for a decrease in uncertainty. These results once again confirm the superiority of the proposed LoUQAL scheme over conventionally used UQ-AL schemes.

Conclusion

In this work, a novel low-fidelity informed uncertainty measure, LoUQ, was introduced and benchmarked for the prediction of different QC properties including the challenging excitation energies. The method was shown to be robust and effective in comparison to existing UQ-AL schemes and the random sampling of molecular configuration space. The performance of this novel method is a key insight into the successful use of AL methods in the ML-QC pipeline. Future cases can readily utilize this approach to efficiently sample the configuration space with guaranteed reduction of empirical error as evidenced by the calibration curves. The computation of the low fidelity QC properties comes at a much cheaper cost (by definition of high and low fidelity) than the computation of the target fidelity thereby making this proposed method attractive. The benchmarks of diverse QC properties for three distinct datasets makes this work of interest to a wide range of users in the ML-QC regime.

LoUQAL is certainly one step in the direction of more meaningful ways to improve and speed up the ML-QC pipeline. One major challenge in the iterative AL scheme used in this work is the repeated predictions over the AL pool data. For a very large dataset with a few million data-points, this would often become regressive, of course this is a challenge with any AL scheme and not limited to the LoUQAL method. One potential solution to this overarching issue is the use of low rank approximations to reduce the computational complexity of needing to perform repeated training and evaluations with the GPR model. An extension of this work could involve applying the LoUQAL method to NN-architecture based ML models for QC such as SchNET [30, 31] or ANI [32, 33].

Figures

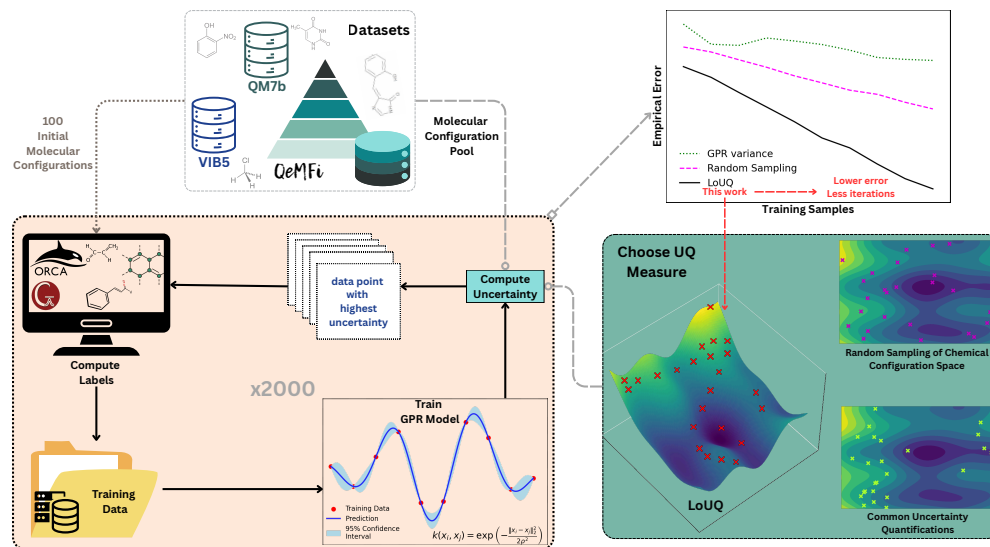


Fig. 1 A pictorial representation of the workflow employed to perform experiments in this work. The computational experiments are performed for three datasets, QM7b [23], VIB5 [24], and QeMFi [25] for diverse QC properties. An initial set of molecular configurations are chosen to train the GPR model after making computations of the QC properties (or labels). This trained model is used to estimate the uncertainty for the unlabeled molecular configurations (AL data pool). The configuration with the highest uncertainty is chosen to be added to the training dataset with the label computed for this configuration. This process is iteratively carried out for different UQ measures. The novel LoUQ measure outperforms the standard measures in both empirical error and number of iterations it takes to reach a specific empirical error.

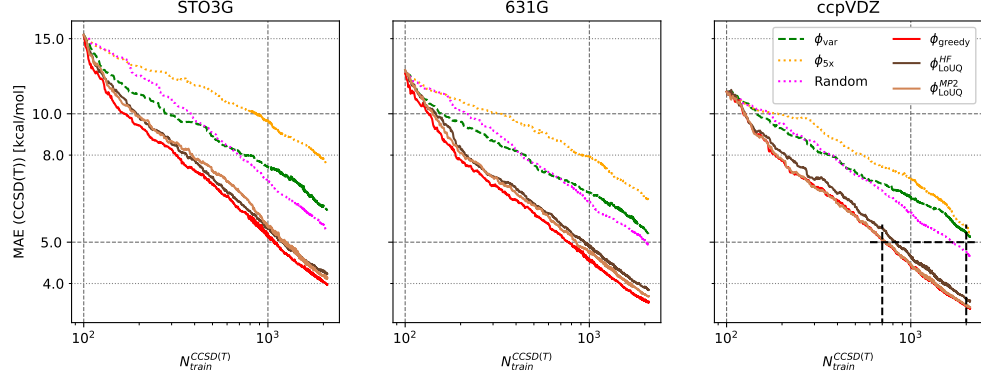


Fig. 2 Learning curves for the prediction of atomization energies of the QM7b dataset with different UQ measures used in the AL scheme. For LoUQ, the low-fidelities are expressed by the choice of the QC method with each pane showing a different basis set choice. Thus, the target fidelity is CCSD(T)-basis with the lower fidelities being HF-basis and MP2-basis.

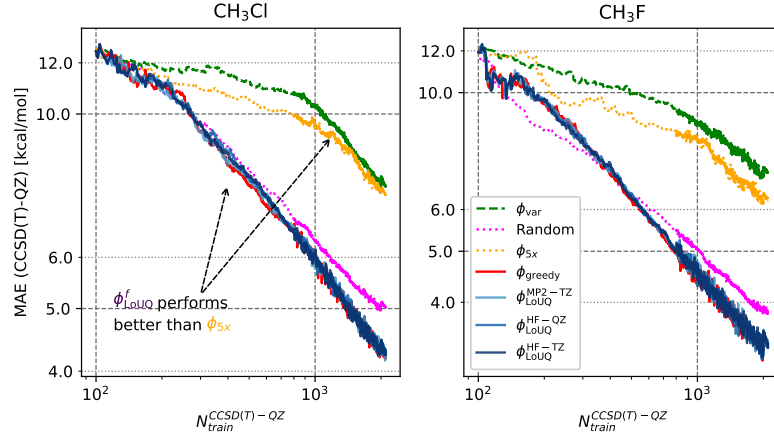


Fig. 3 Learning curves denoted MAE versus number of training samples for the prediction of *ab initio* PES for CH₃Cl and CH₃F from the VIB5 database. Different UQ measures are used for each learning curve shown. The LoUQ measure results in MAEs that are near identical to the greedy adaptive sampling approach.

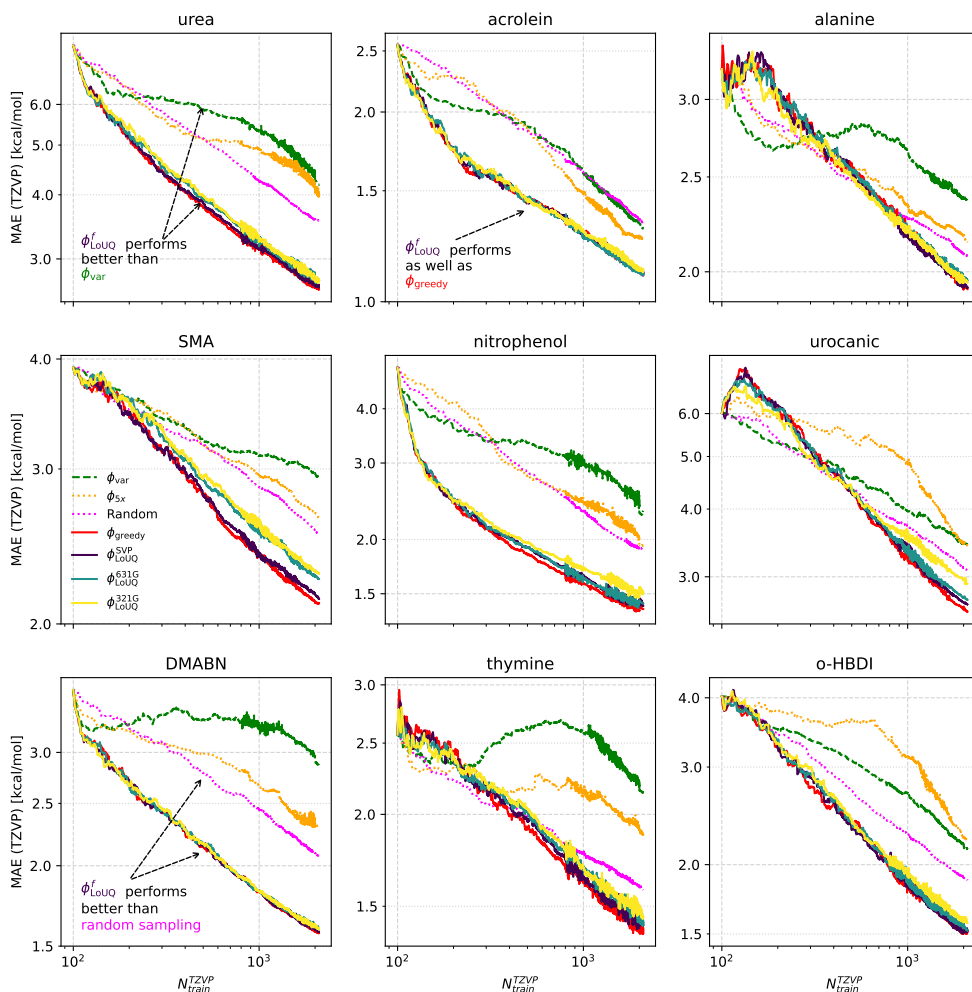


Fig. 4 Learning curves for the prediction of excitation energies of diverse molecules from the QeMFi dataset using GPR. Each data point is added after a cycle of AL with the appropriate UQ measure being employed. The method developed in this work is marked as LoUQ with the terms in the parenthesis indicating the fidelity, in this case corresponding to the basis set chosen. The random sampling approach is also shown for contrast to the approach that is followed in general ML-QC workflows. In every case, the LoUQAL method performs better than other UQ measure based AL schemes.

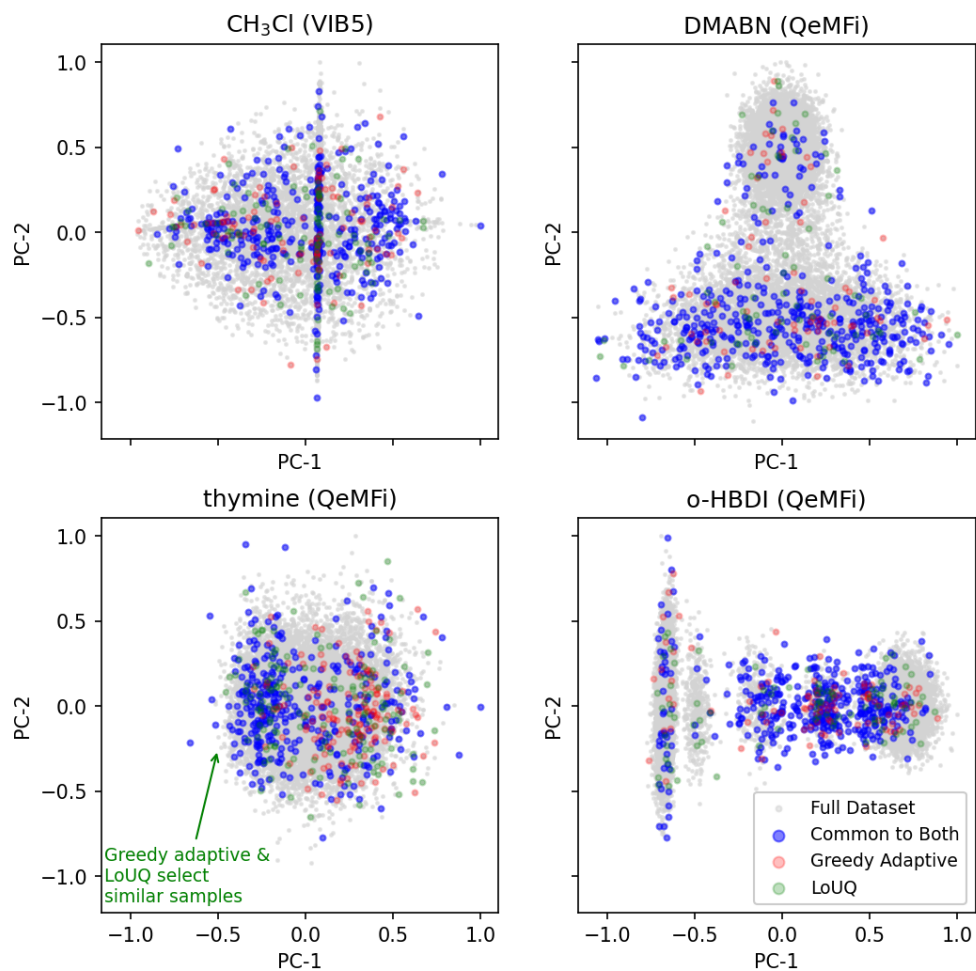


Fig. 5 PCA scatter plot for select molecules studied in this work indicating points selected by the ϕ_{greedy} -AL and LoUQAL approaches in the first 500 iterations. Points selected by both methods are indicated separately. The axes are scaled to lie with unitary values for each principle component. The LoUQAL model selects almost all the same data points as the ϕ_{greedy} -AL model indicating that this is indeed a robust method for configuration space sampling.

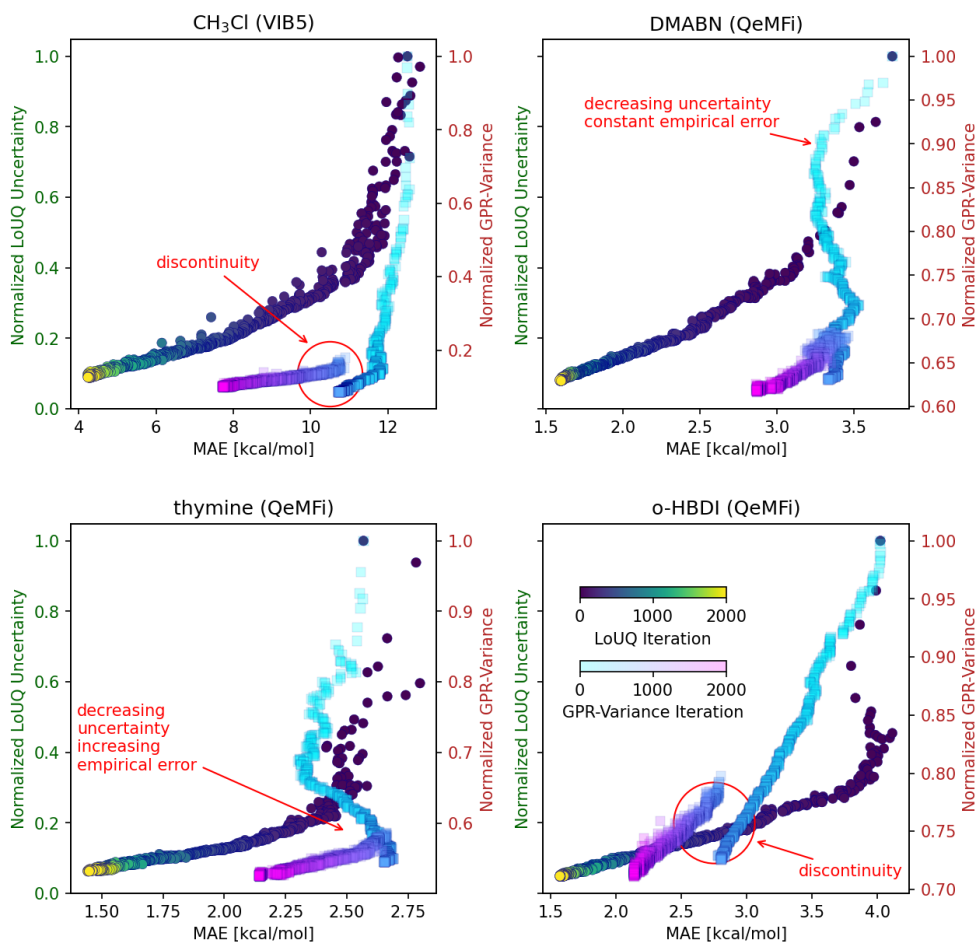


Fig. 6 UQ measures versus empirical error, computed as MAE, of the trained GPR model over the holdout test set for selected molecules from the datasets used in this work. These curves are also referred to as *calibration curves*. The color-scheme of the points correspond to the iteration of the AL scheme. Both the LoUQ and GPR-variance as UQ are reported in normalized units. The left axis corresponds to LoUQ while the right axis corresponds to the GPR-variance. The curves for CH₃Cl correspond to the prediction of *ab initio* ground state PES while the QeMFi molecules correspond to the prediction of DFT excitation energies.

Methods

This section introduces the key online methods employed in this work including the different uncertainty measures that are studied. Details about datasets and molecular descriptors used are presented in the Supplementary Information section S1.

Gaussian Process Regression

Consider the training dataset denoted by $\mathcal{T} := \{(\mathbf{x}_i, y_i^f)\}_{i=1}^{N_{\text{train}}}$ where the inputs are $\mathbf{x}_i \in \mathcal{X} \subseteq \mathbb{R}^D$ and outputs are $y_i^f = g^f(\mathbf{x}_i) \in \mathbb{R}$ computed at some fidelity f . One can collect all the input features from the training dataset into \mathbf{X} and the corresponding outputs into \mathbf{Y} . Let us further define the Gaussian covariance function as

$$k(\mathbf{x}, \mathbf{x}') = \exp\left(-\frac{\|\mathbf{x} - \mathbf{x}'\|_2^2}{2\rho^2}\right), \quad (1)$$

where the term ρ is a length-scale parameter for the covariance function. The covariance function is often also called the kernel function.

Gaussian Process Regression (GPR) is a *non-parametric* ML method which assumes that the relationship between the input to the ML model and the predicted output is a probability distribution over functions defined by a Gaussian process (GP) [10]. The relationship between \mathbf{X} and \mathbf{Y} can be modeled as

$$\mathbf{Y} = \hat{g}^f(\mathbf{X}) + \epsilon, \quad (2)$$

with $\hat{g}^f(\mathbf{X}) = \mathbf{X}^\top \boldsymbol{\omega}$ where $\boldsymbol{\omega}$ is a vector of parameters of the linear model. Furthermore, $\epsilon \sim \mathcal{N}(0, \sigma_{N_{\text{train}}}^2)$, that is, the error is Gaussian distributed with zero mean and constant variance dependent on the training data.

The prediction from a GPR model for a query input feature \mathbf{x}_q is given as

$$\hat{g}^f(\mathbf{x}_q) = \mathbf{K}_q + (\mathbf{K} + \sigma_{N_{\text{train}}}^2 \mathbf{I})^{-1} \mathbf{Y}, \quad (3)$$

where $(\mathbf{K}_q)_i = k(\mathbf{x}_q, \mathbf{x}_i)$, and $(\mathbf{K})_{ij} = k(\mathbf{x}_i, \mathbf{x}_j)$ with i and j indexing the input features in \mathcal{T} . In this work, the GPR process is implemented using the `GPYtorch` library of python [34].

Uncertainty Quantification for Active Learning

Consider the collection of all input features available to a user to build a ML model, denoted by \mathcal{U} . For the applications considered in this work, this would be the collection of all molecular configurations available. It is important to note that the corresponding outputs (or labels) are not yet calculated; having the labels for each input in \mathcal{U} would render the ML pipeline redundant. The aim of AL is to find the best way to select $\mathbf{x} \in \mathcal{X} \subset \mathcal{U}$ to build up the training dataset \mathcal{T}^F at the target fidelity F . A more detailed discussion including the general algorithm for AL is discussed in the Supplementary Information section S1.1. Note that if $\mathcal{U} = \mathcal{X}$, it would render the ML

pipeline redundant since the QC property is now known for all molecular configurations. The optimal selection of training data points would result in an ML model with certain desired qualities such as low empirical error. One strategy used in AL is to compute the uncertainty that arises from a specific choice of training data samples. Uncertainty quantification (UQ) is usually an *a priori* approach in AL in that one does not need the labels for all the inputs in \mathcal{U} .

For this work, two common UQ measures are evaluated along with a random selection approach in contrast to the newly developed UQ measure. The random sampling scheme is the most common approach in ML methods and serves as the control experiment for this work and quantifies the effect of not using AL schemes. Once a UQ measure, denoted by ϕ , is computed for the entire pool of molecular configurations in \mathcal{U} , the optimal selection for the current iteration of AL is carried out with

$$\mathbf{x}_{\text{opt}} = \arg \max_{\mathbf{x} \in \mathcal{U}} \phi(\mathbf{x}) , \quad (4)$$

following which the corresponding QC property is evaluated the training dataset is extended as $\mathcal{T} \cup (\mathbf{x}_{\text{opt}}, g(\mathbf{x}_{\text{opt}}))$.

Variance of the predictive distribution

Consider the query input, \mathbf{x}_q . For a GPR model described in [Gaussian Process Regression](#), the standard deviation of the predictive distribution for \mathbf{x}_q is given by

$$\phi_{\text{var}}(\mathbf{x}_q) = k(\mathbf{x}_q, \mathbf{x}_q) - \mathbf{K}_q^\top (\mathbf{K} + \sigma_n^2 \mathbf{I})^{-1} \mathbf{K}_q \quad (5)$$

where $(\mathbf{K}_q)_i = k(\mathbf{x}_q, \mathbf{x}_i)$ with i indexing the input features in \mathcal{T} . This is often the most common UQ measure for kernel based ML models such as GPR.

Bootstrap Aggregation Ensemble

The bootstrap aggregation ensemble approach is another common UQ for ML models, particularly for neural network based architectures [35, 36]. The notion is to first train an ensemble of n ML models trained on randomly selected subsets of the training data. The uncertainty measure for a query input \mathbf{x}_q is computed as

$$\phi_{n \times}(\mathbf{x}_q) = \sqrt{\frac{1}{N_{\text{ensemble}} - 1} \sum_{l=1}^{N_{\text{ensemble}}} (\hat{g}_l(\mathbf{x}_q) - \bar{g}(\mathbf{x}_q))^2} , \quad (6)$$

where

$$\bar{g}(\mathbf{x}_q) = \frac{1}{N_{\text{ensemble}}} \sum_{b=1}^{N_{\text{ensemble}}} \hat{g}_b(\mathbf{x}_q) , \quad (7)$$

that is, the mean prediction of the different models in the ensemble. In short, the UQ measure is the standard deviation of the prediction of the ensemble. Note that the division by $N_{\text{ensemble}} - 1$ ensures this is an unbiased estimator for the standard

deviation, particularly for small $N_{\text{ensembles}}$. In this work, a 5-fold ensemble is used, that is 5 different ML models are trained, and therefore the UQ measure is denoted as $\phi_{5\times}$ in the manuscript. Each of the model in the ensemble uses 85% of the total training set available each AL iteration. This ensures that the ML models trained in this scheme do not suffer significantly in terms of number of training samples in comparison to the other UQ measures which have access to 100% of the training samples per AL iterations.

Low-fidelity informed Uncertainty Quantification

Assume an ordered hierarchy of fidelities denoted as $f \in \{1, 2, \dots, F-1\}$ with F being the *target fidelity*, that is the most accurate (and by extension, expensive) fidelity. The Low-fidelity informed Uncertainty Quantification (LoUQ) for a query descriptor, \mathbf{x}_q , is computed as the absolute difference in prediction and reference of the output property:

$$\phi_{\text{LoUQ}}^f(\mathbf{x}_q) = |\hat{g}^f(\mathbf{x}_q) - g^f(\mathbf{x}_q)|, \quad (8)$$

where f denotes the fidelity used for the reference computations. In this work, the impact of using different fidelities f on empirical error are studied. In such a notion, $f = 1$ has a ‘larger distance’ from F than $f = 2$ and so on.

Greedy Adaptive Sampling

The greedy adaptive sampling method, unlike the other UQ measures in this work, does not work on an *a priori* notion. Rather, it explicitly requires that the labels be computed for all $\mathbf{x} \in \mathcal{U}$. This method is studied here as the best possible UQ measure for AL. The argument is that if one had complete knowledge of how the function g looked like, how would one go about selecting training samples. This method is yet another control experiment in that all UQ-AL schemes attempt to get closest to the robustness offered by this scheme. The novel method, LoUQAL, developed herein performs as well as the greedy adaptive sampling scheme for AL.

Formally, consider that the reference output is computed for each $\mathbf{x} \in \mathcal{U}$ at fidelity F , the target fidelity. Then the UQ for greedy adaptive sampling for some query input feature \mathbf{x}_q is defined as

$$\phi_{\text{greedy}}(\mathbf{x}_q) = |\hat{g}^F(\mathbf{x}_q) - g^F(\mathbf{x}_q)|. \quad (9)$$

Notice that setting $f = F$ defaults ϕ_{LoUQ} to ϕ_{greedy} .

Random Sampling

In general ML approaches, the most common approach to selecting training samples is by randomly sampling across the entire pool of data to build the training dataset \mathcal{T} . Although this approach is technically not an uncertainty informed method, it is still relevant to understand this process in order to evaluate the results of this work. Indeed, this method is the control experiment without any AL strategy involved. Formally,

this approach proposes selecting a data point from the AL data pool with probability

$$p(\mathbf{x}) = \begin{cases} \frac{1}{|\mathcal{X}|}, & \text{if } \mathbf{x} \in \mathcal{X} \\ 0, & \text{otherwise} \end{cases}, \quad (10)$$

where $|\mathcal{X}|$ is the cardinality of the data pool, or specific to this work, the number of molecular configurations available in the data pool. This can also be interpreted as each molecular configuration $\mathbf{x} \in \mathcal{U}$ being assigned a fixed uncertainty.

Error Metrics

ML models that are produced as a result of the different AL schemes proposed in this work are evaluated on the basis of mean absolute error (MAE) over a holdout test set $\mathcal{V} := \{(\mathbf{x}_t, y_t^F)\}_{t=1}^{N_{\text{test}}}$ where $y_t^F = g^F(\mathbf{x}_t)$ is computed at the target fidelity F . This test set is not used in any of the training phases. For each case, the MAE is computed using a discrete L_1 norm as follows:

$$\text{MAE} = \frac{1}{N_{\text{test}}} \sum_{t=1}^{N_{\text{test}}} |\hat{g}^F(\mathbf{x}_t^{\text{test}}) - y_t^F|. \quad (11)$$

The MAE is always computed with reference to the target fidelity QC properties. The evolution of MAE with increasing model complexity is studied as the learning curve and indicates how well an ML model is able to predict over unseen data [37]. For GPR, model complexity is explicitly dependent on number of training samples used. Therefore, in this work, MAE versus number of training samples used are studied in order to make inferences about the ability of a GPR model in predicting properties for inputs from \mathcal{V} .

Code and Data availability

The programming scripts used for this work can be openly accessed at the [LoQUAL-for-QC](#) GitHub repository. All data used in this work comes from openly available datasets which are appropriately cited.

Supplementary information

Supplementary sections S1-S2, figures SF1-SF2, algorithms SA1-SA3.

Acknowledgments

The authors acknowledge support by the DFG through the project ZA 1175/3-1 as well as through the DFG Priority Program SPP 2363 on ‘‘Utilization and Development of Machine Learning for Molecular Applications – Molecular Machine Learning’’ through the project ZA 1175/4-1. The authors would also like to acknowledge the support of the ‘Interdisciplinary Center for Machine Learning and Data Analytics (IZMD)’ at the University of Wuppertal.

Declarations

The authors declare that there is no conflict of interest or any competing interests.

Supplementary Information for LoUQAL

S1 Supplementary Methods

S1.1 Active Learning

Algorithm SA1 Active Learning by Uncertainty Sampling for single fidelity approach.

Require: AL pool of input features \mathcal{U} , number of AL iterations n_{iter} , initial number of training samples n_{init}

```
1:  $\mathcal{A} \leftarrow$  Randomly select  $n_{\text{init}}$  samples from  $\mathcal{U}$ 
2:  $\mathbf{Y} \leftarrow y_i^f = g^f(\mathbf{x}_i), \forall \mathbf{x}_i \in \mathcal{A}$  ▷ Compute output at fidelity  $f$ 
3:  $\mathcal{U} \leftarrow \mathcal{U} \setminus \mathcal{A}$ 
4:  $\mathcal{T} \leftarrow \{\mathcal{A}, \mathbf{Y}\}$ 
5: Train initial model  $M_{\mathcal{T}}$ 
6: for  $i = 1$  to  $n_{\text{iter}}$  do
7:    $\Phi \leftarrow [\phi(\mathbf{x}_q)]_{\mathbf{x}_q \in \mathcal{U}}$  ▷ Compute uncertainty measure  $\phi$ 
8:    $\text{ind}_{\text{opt}} \leftarrow \arg \max_{\mathbf{x}} \Phi(\mathbf{x})$ 
9:    $\mathbf{x}_a \leftarrow \mathcal{U}[\text{ind}_{\text{opt}}]$  ▷ Identify  $\mathbf{x}_q$  with highest uncertainty
10:   $y_a \leftarrow g^f(\mathbf{x}_a)$ 
11:   $\mathcal{A} \leftarrow \mathcal{A} \cup \mathbf{x}_a$ 
12:   $\mathcal{U} \leftarrow \mathcal{U} \setminus \mathcal{A}$ 
13:   $\mathbf{Y} \leftarrow \mathbf{Y} \cup y_a$ 
14:   $\mathcal{T} \leftarrow \{\mathcal{A}, \mathbf{Y}\}$  ▷ Update training set
15:  Retrain  $M_{\mathcal{T}}$ 
16: end for
17: return Trained model  $M_{\mathcal{T}}$ 
```

Active learning is a class of methods in ML that attempt to make a well informed decision on how to select optimal training samples for the Active learning (AL) algorithms try to choose new training samples, which are maximally informative to an ML model. In our setup, we have a large amount of unlabeled molecular configurations and generating the respective labels (excitation energies) via quantum chemical calculations is expensive. For this setting, UQ sampling [38] can be a well suited AL scheme. The process of performing AL using UQ sampling is delineated in Algorithm SA1. An initial ML model is trained using training data chosen randomly from the entire data pool (denoted by \mathcal{U}). Each iteration of the AL algorithm computes the UQ measure, ϕ , for the samples $\mathbf{x}_q \in \mathcal{U}$ following which the \mathbf{x}_q with the highest uncertainty is added to the training dataset after computing the reference output property. Finally, the trained ML model is returned for use.

S1.2 A Note on Fidelities

Fidelity, as the term suggests, is a measure of how close one is to the notion of ground truth. In computation QC, there is often a clear hierarchy of fidelities, that is, each method of computational QC comes with a cost and accuracy attached to it. For instance, Coupled Cluster Singles Doubles (Triples), abbreviated CCSD(T), is considered the gold standard in QC methods [39, 40] which scales as $\mathcal{O}(O^2 \cdot N^8)$ with N being number of basis functions and O representing occupied orbitals being considered. The high accuracy of CCSD(T) comes with a high computational cost, making it a high fidelity method. In contrast, methods like density functional theory (DFT) or Møller–Plesset perturbation theory (MP2) are considered to be cheaper and less accurate, therefore being low fidelity methods [41–43].

S1.3 Datasets

This work employs several datasets in order to assess the effect of using LoFiAL over other uncertainty measure informed AL. While these are well known datasets, for completeness, key details of these datasets are mentioned here.

S1.3.1 QM7b

The QM7b dataset is a collection of 7211 molecules with several heavy atoms including C, N, and O [23]. The dataset provides the atomization energies of these molecules, that is, the measure of energy required to break a molecule into unbound atoms. The energies are calculated with the Hartree Fock (HF) [44, 45], Møller–Plesset perturbation theory (MP2) [41, 43, 46] [39, 40, 47], and Coupled Cluster Singles and Doubles perturbative Triples (CCSD(T)). For each method, three basis set sizes are used for computation, STO3G, 631G, and ccpVDZ. Therefore, there are a total of 9 point calculations made for each molecule in this dataset. The most expensive method, or fidelity, is the CCSD(T) method with the cc-pVDZ basis set, hereon denoted as CCSD-ccpVDZ. Similarly, each method and basis set is hereon concatenated in reference such as HF-STO3G.

S1.3.2 VIB5

The VIB5 database contains high accuracy *ab initio* potential energy surfaces (PES) for several small molecules such as CH_3Cl and CH_3F [24]. For these two molecules, there are 44,819 and 82,653 point geometries respectively. This was achieved by performing an energy-weighted Monte Carlo sampling strategy to internal coordinates of the molecules such as the X-C-H bond angles (X represents the halogen), dihedral angles, and bond lengths between C and constituent atoms. Corresponding energies are computed with varying degrees of accuracy. The fidelities used in this work are the CCSD(T)-ccpVQZ, MP2-ccpVTZ, HF-ccpVQZ, and HF-ccpVTZ. The target fidelity assumed is the CCSD(T)-ccpVQZ for both molecules.

S1.3.3 QeMFi

The quantum chemistry multifidelity (QeMFi) dataset [25, 29] consists of nine chemically diverse molecules with varying sizes with QC properties computed with the DFT formalism [25, 29]. These molecules include 2-(methylinomethyl)phenol (SMA), 4-(dimethylamino) benzonitrile (DMABN), and 4-(2-hydroxybenzylidene)-1,2-dimethyl-1H-imidazol-5(4H)-one (o-HBDI). For each of the nine molecules, excitation energies are computed with the DFT *ansatz* using the CAM-B3LYP functional. The fidelities available in this dataset are ordered by the size of the basis set used, namely, STO3G, 321G, 631G, def2-SVP, and def2-TZVP. The energies are computed for $9 \times 15,000$ geometries. In this work, the various AL strategies are assessed for individual molecules of the QeMFi dataset for different f_b baseline fidelities. However, STO3G is omitted since it was identified in previous works with QeMFi as a fidelity with poor characteristics [48, 49].

S1.4 Molecular Descriptors

Intermediate steps in the ML-QC pipeline involve making the choice of *molecular descriptors* or *representations* which are mappings between the Cartesian coordinates of the molecular configurations to machine learnable input features [50, 51]. Often, QC details of the molecule of interest are also included such as the nuclear charge or tetrahedral bond angles. Several representations are actively used in the ML-QC workflow. These include Coulomb Matrices (CM) [28], smooth overlap of atomic positions (SOAP) [50], the spectrum of London and Axilrod-Teller-Muto (SLATM) representation [26], atom-centered symmetry functions (ACSFs) of Behler [33, 52, 53], and the Faber-Christensen-Huang-Lilienfeld (FCHL) descriptor [54].

One of the molecular descriptors used in this work are the simple unsorted Coulomb Matrix (CM) [28]. For a molecule whose atoms are indexed by i with corresponding nuclear charge Z_i , these are computed as

$$C_{i,j} := \begin{cases} \frac{Z_i^{2.4}}{2}, & i = j \\ \frac{Z_i \cdot Z_j}{\|\mathbf{R}_i - \mathbf{R}_j\|}, & i \neq j, \end{cases} \quad (\text{S1})$$

where the Cartesian coordinates of an atom are given by \mathbf{R}_i and the computation is performed for all pairs of atoms. The CM is a symmetric representation and therefore is of size $n(n-1)/2$ for a molecule with n atoms. The experiments for QeMFi and VIB5 are performed using this descriptor.

For the atomization energies of the QM7b dataset, since there are several different molecules as opposed to a single molecule as for the case of VIB5 or QeMFi, the unsorted CM descriptors fail in terms of permutational invariance. Furthermore, the use of CM matrices sorted by their row norm is known to introduce discontinuities in the learned function [28, 55]. Therefore, this descriptor is avoided. Instead, based on previous work with this dataset in refs. [56, 57] the SLATM representation [26] is used.

S1.5 Hyper-parameter Optimization

The hyperparameters for each of the GPR models built in this cases were optimized with the initial training data chosen before performing any AL. In order to do so, the exact marginal log-likelihood (MLL) was minimized using an ADAM optimizer as provided by the `GPYtorch` package. Algorithm SA2 describes the computation of the MLL for a given GPR model with a choice of hyper-parameters. At the same time, the entire process of hyper-parameter optimization as implemented for this work is described in Algorithm SA3. Once hyper-parameters are trained with the initial training data, they are not optimized any time along the AL iterations.

Algorithm SA2 Exact Marginal Log-Likelihood (MLL) Computation for GPR

Require: GPR model M_θ , Likelihood L , Validation set $\mathcal{K} := \{(\mathbf{x}_i, y_i)\}_{i=1}^{N_{\text{val}}}$.

- 1: $\boldsymbol{\mu} = M_\theta(\mathbf{X})$ \triangleright predictions with M_θ for inputs features in \mathcal{K} with parameters θ
- 2: $\mathbf{K}_\mathcal{K}$ covariance matrix of $M_\theta(\mathbf{X})$
- 3: $\mathbf{K}_{\text{noisy}} = \mathbf{K}_\mathcal{K} + \mathbf{K}_{\text{noise}}$
- 4: $\tilde{\mathbf{y}} = \mathbf{y} - \boldsymbol{\mu}$ $\triangleright N$ is the dimension of \mathbf{y}
- 5: $\mathcal{L}_{MLL} = -\frac{1}{2}\tilde{\mathbf{y}}^T \mathbf{K}_{\text{noisy}}^{-1} \tilde{\mathbf{y}} - \frac{1}{2} \log(|\mathbf{K}_{\text{noisy}}|) - \frac{N}{2} \log(2\pi)$
- 6: **return** \mathcal{L}_{MLL}

Algorithm SA3 Hyperparameter Training for GPR using MLL

Require: GPR model M_θ (Hyperparameters θ), Likelihood L , Validation set \mathcal{K} , Learning Rate r , Maximum Iterations n_{maxiter} , Convergence Tolerance τ .

- 1: Initialize optimizer for model and likelihood parameters with r
- 2: Initialize empty list *losses*
- 3: **for** $i = 1$ to n_{maxiter} **do**
- 4: Clear gradients
- 5: Compute model output $\hat{\mathbf{y}}$ for validation inputs \mathbf{X}_{val}
- 6: $\mathcal{L} = -\text{MLL}(\hat{\mathbf{y}}, \mathbf{y}_{\text{train}})$ \triangleright Compute negative Marginal Log-Likelihood (MLL)
- 7: Back-propagate gradients
- 8: Update model and likelihood parameters using optimizer
- 9: Add current \mathcal{L} to *losses*
- 10: **if** $|\mathcal{L}_i - \mathcal{L}_{i-1}| < \tau$ **then**
- 11: Break loop \triangleright Change in loss tolerance condition
- 12: **end if**
- 13: **end for**
- 14: **return** Model hyperparameters θ

S1.6 Principle Component Analysis

PCA is a common dimensionality reduction approach that helps in visualizing high dimensional input data in order for visual intuition of patterns in data. In this work, PCA is used only as a secondary tool to understand the effect of using different uncertainty measures from the main text. Consider the input features collected into \mathbf{X} from the previous sections. With PCA, one is interested in finding k *principle components*, that is k orthonormal vectors. All $\mathbf{x} \in \mathbf{X}$ can be represented as a linear combination of these k vectors. Formally, given centered \mathbf{x}_i , PCA provides the model

$$\hat{f}_k(\boldsymbol{\beta}) = \hat{\mathcal{H}}_k \boldsymbol{\beta} , \quad (\text{S2})$$

with $\boldsymbol{\beta} = (\boldsymbol{\beta}^{(1)}, \dots, \boldsymbol{\beta}^{(k)})^\top$ and

$$\hat{\mathcal{H}}_k = \arg \min_{\mathcal{H}_k} \sum_{i=1}^{N_{\text{train}}} \|\mathbf{x}_i - \mathcal{H} \mathcal{H}^\top \mathbf{x}_i\|_2^2 . \quad (\text{S3})$$

Each \mathbf{x}_i can then be approximated with

$$\hat{\mathbf{x}}_i = \hat{\mathcal{H}} \hat{\mathcal{H}}^\top \mathbf{x}_i . \quad (\text{S4})$$

PCA is used in main text in order to study which points in the input feature space are chosen by the different uncertainty measures used for AL in this work.

S2 Supplementary Results

Additional results that accompany the main text are presented in this section.

S2.1 Composite fidelity effect on LoUQAL

Another comprehensive way to test the robustness of the LoFiAL approach is shown in Fig. SF1. In this case, the most expensive fidelity is CCSD(T)-ccpVDZ. Every other fidelity such as MP2-631G or HF-STO3G are considered cheap fidelities. The aim with LoFiAL here is to see how much the choice of QC method *and* basis set have on the MAE of the model. Once again, the comparison with GPR-variance, random sampling, and greedy approach is shown. Note that this time around, the notion of a fidelity is a combination of both the method and the basis set choice. While the LoFiAL method with cheaper fidelities does indeed provide a better MAE than the GPR-variance and random sampling approach, there is a varying degree of improvement that is seen as the chosen lower fidelity gets farther away from CCSD(T)-ccpVDZ. An observation can be made that the basis set choice seems to make more of a difference than the QC method chosen. For instance, the model built with LoFiAL (MP2-ccpVDZ) performs much better than that built with LoFiAL (CCSD(T)-STO3G). This observation can be understood better from the perspective that the choice of a basis set is the notion of where the wave function is truncated. The choice of truncation could potentially play a stronger role in the LoFiAL method than the specific QC method. Regardless,

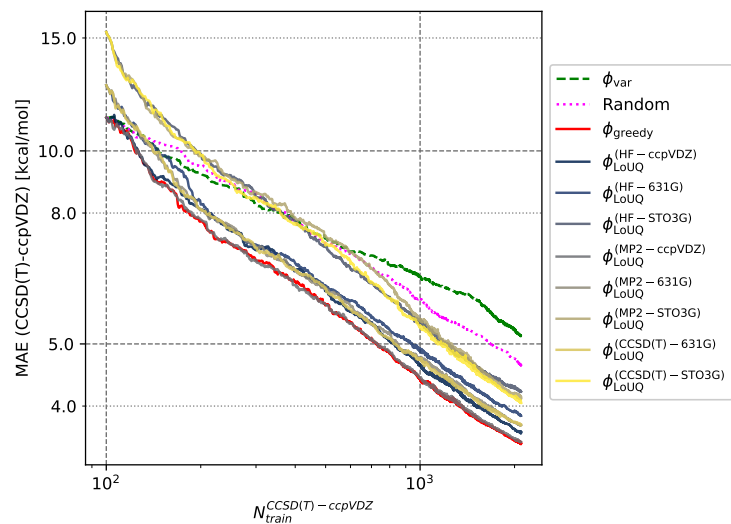


Fig. SF1 Learning curves for AL strategies for the prediction of atomization energies of the QM7b dataset where the target fidelity is fixed as CCSD(T)-ccpVDZ and the remaining fidelities are used to perform LoUQAL.

it is observed that the LoFiAL method is able to get close to the greedy sampling method in this case.

S2.2 PCA For GPR-variance as UQ measure

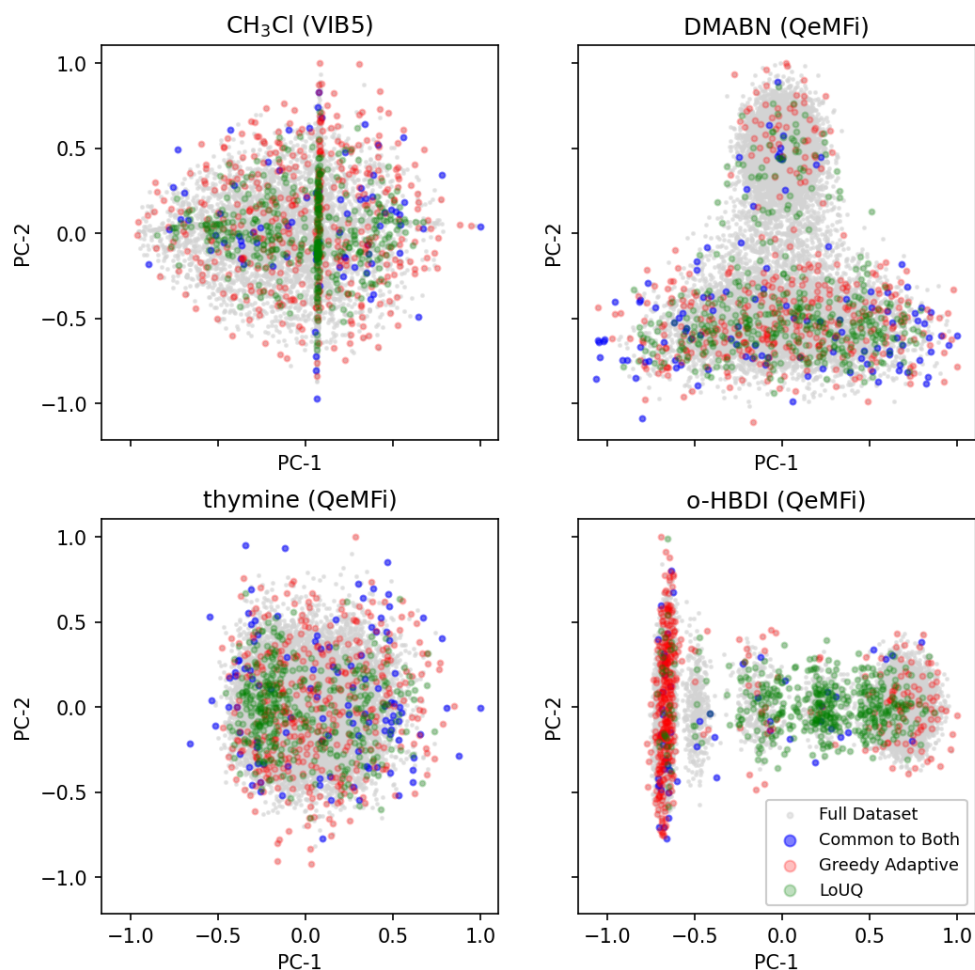


Fig. SF2 PCA scatter plot for selected molecules studied in this work indicating points selected by ϕ_{var} and ϕ_{LoUQ} UQ measures in the first 500 iterations of AL. Those points selected by both methods are indicated separately. The axes are scaled to lie with unitary values for each principle component. The GPR-variance based AL places more importance to the peripheral regions of the scatter plots while the LoUQAL approach shows more concentrated selection of data points across all the four molecules.

Fig. SF2 depicts the PCA scatter plot for 3 specific molecules: CH₃Cl from VIB5, and nitrophenol and DMABN from QeMFi. For these molecules, the 2-D PCA of the entire 15,000 samples is depicted in the background. The scatter plots include three distinct groups of points. Those data points selected using GPR-variance as uncertainty, those

selected in LoUQAL, and finally those common to both. Only the first 500 samples that were chosen, that is the first 500 iterations of AL, are shown in order to have a less cluttered view of the PCA plots. The PCA plots are only shown for the AL pool and not for the initial training data and holdout test set.

In all three cases, it can be observed that there are rather few samples that are common to the two different uncertainty measures. The two methods do indeed seem to sample distinct parts of this proxy space. Consider the case for CH_3Cl . The LoUQAL (HF-TZ) method is shown. The GPR-variance AL approach has an almost even sampling of the proxy space with points at the periphery of the scatter plot being strongly considered. In contrast, the LoUQAL approach seems to concentrate in the + shaped central beams with some deviations around this structure. The peripheral structure of the proxy space does not seem to be of great importance to this selection strategy.

For the case of nitrophenol, as seen in the middle scatter plot of Fig. SF2, the PCA depicts 2 major clusters with 3 minor clusters in between them. The GPR-variance based AL method samples sparingly on the left-side cluster and samples evenly from the right-most cluster. Once again this method picks data points that are at the edge of the proxy-space. In contrast, the LoUQAL method, here shown for the 321G fidelity samples concentrated at the left side cluster and a more narrower sampling on the right-most cluster. A similar observation is made for DMABN where the LoUQAL (321G) method samples less on the top cluster in comparison to the GPR-variance AL method.

The observations of the PCA plots from Fig. SF2 can be understood by noticing that the GPR-variance computed using Eq. (5) is based purely on the input feature space and has no information about the QC property landscape. This leaves it at a disadvantage. The use of low fidelity QC properties allows for the LoUQAL method incorporates some information about how the property of interest looks like. This allows it to perform a more meaningful sampling for training samples from the data pool.

References

- [1] Behler, J.: Constructing high-dimensional neural network potentials: a tutorial review. *Int. J. Quantum Chem.* **115**(16), 1032–1050 (2015) <https://doi.org/10.1002/qua.24890>
- [2] Butler, K.T., Davies, D.W., Cartwright, H., Isayev, O., Walsh, A.: Machine learning for molecular and materials science. *Nature* **559**(7715), 2336–2347 (2018) <https://doi.org/10.1038/s41586-018-0337-2>
- [3] Baum, Z.J., Yu, X., Ayala, P.Y., Zhao, Y., Watkins, S.P., Zhou, Q.: Artificial intelligence in chemistry: Current trends and future directions. *J. Chem. Inf. Model.* **61**(7), 3197–3212 (2021) <https://doi.org/10.1021/acs.jcim.1c00619>
- [4] Dral, P.O.: Quantum chemistry in the age of machine learning. *J. Phys. Chem. Lett.* **11**(6), 2336–2347 (2020) <https://doi.org/10.1021/acs.jpcllett.9b03664>

- [5] Schwaller, P., Laino, T.: 4. Data-Driven Learning Systems for Chemical Reaction Prediction: An Analysis of Recent Approaches, pp. 61–79. ACS, 1155 Sixteenth Street N.W., Washington, DC 20036 (2019). <https://doi.org/10.1021/bk-2019-1326.ch004>
- [6] Häse, F., Valleau, S., Pyzer-Knapp, E., Aspuru-Guzik, A.: Machine learning exciton dynamics. *Chem. Sci.* **7**(8), 5139–5147 (2016) <https://doi.org/10.1039/C5SC04786B>
- [7] González, L., Lindh, R. (eds.): *Quantum Chemistry and Dynamics of Excited States*. Wiley, (2020). <https://doi.org/10.1002/9781119417774>
- [8] White, D.A., Sofge, D.A.: *Handbook of Intelligent Control: Neural, Fuzzy, and Adaptive Approaches*. VNR computer library. Van Nostrand Reinhold, (1992)
- [9] Atlas, L., Cohn, D., Ladner, R.: Training connectionist networks with queries and selective sampling. *Advances in neural information processing systems* **2** (1989)
- [10] Williams, C.K., Rasmussen, C.E.: *Gaussian Processes for Machine Learning* vol. 2. MIT press, 314 Main St, Cambridge, MA 02142 (2006). <https://doi.org/10.7551/mitpress/3206.001.0001>
- [11] Rupp, M., Bauer, M.R., Wilcken, R., Lange, A., Reutlinger, M., Boeckler, F.M., Schneider, G.: Machine learning estimates of natural product conformational energies. *PLoS Comput. Biol.* **10**(1), 1003400 (2014) <https://doi.org/10.1371/journal.pcbi.1003400>
- [12] Uteva, E., Graham, R.S., Wilkinson, R.D., Wheatley, R.J.: Active learning in Gaussian process interpolation of potential energy surfaces. *J. Chem. Phys.* **149**(17) (2018) <https://doi.org/10.1063/1.5051772>
- [13] Guan, Y., Yang, S., Zhang, D.H.: Construction of reactive potential energy surfaces with Gaussian process regression: active data selection. *Mol. Phys.* **116**(7-8), 823–834 (2018) <https://doi.org/10.1080/00268976.2017.1407460>
- [14] Vandermause, J., Torrisi, S.B., Batzner, S., Xie, Y., Sun, L., Kolpak, A.M., Kozinsky, B.: On-the-fly active learning of interpretable Bayesian force fields for atomistic rare events. *Npj Comput. Mater.* **6**(1), 20 (2020) <https://doi.org/10.1038/s41524-020-0283-z>
- [15] Christiansen, M.-P.V., Rønne, N., Hammer, B.: Efficient ensemble uncertainty estimation in gaussian processes regression. *Machine Learning: Science and Technology* **5**(4), 045029 (2024) <https://doi.org/10.1088/2632-2153/ad8984>
- [16] Huang, Y., Hou, Y.-F., Dral, P.O.: Active delta-learning for fast construction of interatomic potentials and stable molecular dynamics simulations. *Mach. Learn.: Sci. Technol.* **6**(3), 035004 (2025) <https://doi.org/10.1088/2632-2153/adeb46>

- [17] Schaback, R., Wendland, H.: Adaptive greedy techniques for approximate solution of large rbf systems. *Numer. Algor.* **24**(3), 239–254 (2000)
- [18] Ling, L., Schaback, R.: An improved subspace selection algorithm for meshless collocation methods. *International journal for numerical methods in engineering* **80**(13), 1623–1639 (2009)
- [19] Holzenkamp, M., Lyu, D., Kleinekathöfer, U., Zaspel, P.: Evaluation of uncertainty estimations for Gaussian process regression based machine learning interatomic potentials (2025). <https://arxiv.org/abs/2410.20398>
- [20] Kuleshov, V., Fenner, N., Ermon, S.: Accurate uncertainties for deep learning using calibrated regression (2018). <https://arxiv.org/abs/1807.00263>
- [21] Levi, D., Gispan, L., Giladi, N., Fetaya, E.: Evaluating and calibrating uncertainty prediction in regression tasks. *Sensors* **22**(15) (2022) <https://doi.org/10.3390/s22155540>
- [22] Garain, B.C., Jr, M.P., Bispo, M.O., Barbatti, M.: Enhancing uncertainty quantification in molecular machine learning: A comparative study of deep evidential regression and ensembles with posthoc calibration (2025). <https://doi.org/10.26434/chemrxiv-2025-fx019>
- [23] Montavon, G., Rupp, M., Gobre, V., Vazquez-Mayagoitia, A., Hansen, K., Tkatchenko, A., Müller, K.-R., Von Lilienfeld, O.A.: Machine learning of molecular electronic properties in chemical compound space. *New J. Phys.* **15**(9), 095003 (2013) <https://doi.org/10.1088/1367-2630/15/9/095003>
- [24] Zhang, L., Zhang, S., Owens, A., Yurchenko, S.N., Dral, P.O.: VIB5 database with accurate ab initio quantum chemical molecular potential energy surfaces. *Sci. Data* **9**(1), 84 (2022) <https://doi.org/10.1038/s41597-022-01185-w>
- [25] Vinod, V., Zaspel, P.: QeMFi: A multifidelity dataset of quantum chemical properties of diverse molecules. *Sci. Data* **12**(1), 202 (2025) <https://doi.org/10.1038/s41597-024-04247-3>
- [26] Huang, B., Lilienfeld, O.A.: Quantum machine learning using atom-in-molecule-based fragments selected on the fly. *Nat. Chem.* **12**(10), 945–951 (2020) <https://doi.org/10.1038/s41557-020-0527-z>
- [27] Lilienfeld, O.A., Ramakrishnan, R., Rupp, M., Knoll, A.: Fourier series of atomic radial distribution functions: A molecular fingerprint for machine learning models of quantum chemical properties. *Int. J. Quantum Chem.* **115**(16), 1084–1093 (2015) <https://doi.org/10.1002/qua.24912>
- [28] Rupp, M., Tkatchenko, A., Müller, K.-R., Lilienfeld, O.A.: Fast and accurate modeling of molecular atomization energies with machine learning. *Phys. Rev. Lett.*

- 108**, 05830–1058305 (2012) <https://doi.org/10.1103/PhysRevLett.108.058301>
- [29] Vinod, V., Zaspel, P.: QeMFi: A multifidelity dataset of quantum chemical properties of diverse molecules (1.1.0) [dataset]. Zenodo (2024) <https://doi.org/10.5281/zenodo.13925688>
 - [30] Schütt, K.T., Sauceda, H.E., Kindermans, P.-J., Tkatchenko, A., Müller, K.-R.: Schnet—a deep learning architecture for molecules and materials. *J. Chem. Phys.* **148**(24), 241722 (2018) <https://doi.org/10.1063/1.5019779>
 - [31] Schütt, K.T., Unke, O.T., Gastegger, M.: Equivariant message passing for the prediction of tensorial properties and molecular spectra (2021). <https://arxiv.org/abs/2102.03150>
 - [32] Gao, X., Ramezanghorbani, F., Isayev, O., Smith, J.S., Roitberg, A.E.: TorchANI: A free and open source pytorch-based deep learning implementation of the ani neural network potentials. *J. Chem. Inf. Modeling* **60**(7), 3408–3415 (2020) <https://doi.org/10.1021/acs.jcim.0c00451>
 - [33] Smith, J.S., Isayev, O., Roitberg, A.E.: ANI-1: An extensible neural network potential with DFT accuracy at force field computational cost. *Chem. Sci.* **8**(4), 3192–3203 (2017) <https://doi.org/10.1039/C6SC05720A>
 - [34] Gardner, J., Pleiss, G., Weinberger, K.Q., Bindel, D., Wilson, A.G.: Gpytorch: Blackbox matrix-matrix Gaussian process inference with GPU acceleration. *Advances in neural information processing systems* **31** (2018)
 - [35] Efron, B.: Bootstrap methods: another look at the jackknife. In: *Breakthroughs in Statistics: Methodology and Distribution*, pp. 569–593. Springer, (1992)
 - [36] Bishop, C.M., Nasrabadi, N.M.: *Pattern Recognition and Machine Learning* vol. 4. Springer, (2006). Pages 147–152
 - [37] Cortes, C., Jackel, L.D., Solla, S.A., Vapnik, V., Denker, J.S.: Learning curves: asymptotic values and rate of convergence. In: *Proceedings of the 6th International Conference on Neural Information Processing Systems. NIPS’93*, pp. 327–334. Morgan Kaufmann Publishers Inc., (1993). <https://doi.org/10.5555/2987189.2987231>
 - [38] Lewis, D.D.: A sequential algorithm for training text classifiers: Corrigendum and additional data. In: *ACM SIGIR Forum*, vol. 29, pp. 13–19 (1995). ACM New York, NY, USA
 - [39] Crawford, T.D., Schaefer III, H.F.: *An Introduction to Coupled Cluster Theory for Computational Chemists*, pp. 33–136. John Wiley & Sons, Ltd, (2000). <https://doi.org/10.1002/9780470125915.ch2>

- [40] Bartlett, R.J., Musiał, M.: Coupled-cluster theory in quantum chemistry. *Rev. Mod. Phys.* **79**, 291–352 (2007) <https://doi.org/10.1103/RevModPhys.79.291>
- [41] Quiñonero, D., Garau, C., Frontera, A., Ballester, P., Costa, A., Deyà, P.M.: Structure and binding energy of anion- π and cation- π complexes: A comparison of mp2, ri-mp2, dft, and df-dft methods. *J. Phys. Chem. A* **109**(20), 4632–4637 (2005) <https://doi.org/10.1021/jp044616c>
- [42] Jensen, F.: *Introduction to Computational Chemistry*, 3rd edition edn. Wiley, (2017)
- [43] Pogrebetsky, J., Siklitskaya, A., Kubas, A.: MP2-based correction scheme to approach the limit of a complete pair natural orbitals space in DLPNO-CCSD(T) calculations. *J. Chem. Theory Comput.* **19**(13), 4023–4032 (2023) <https://doi.org/10.1021/acs.jctc.3c00444>
- [44] Slater, J.C.: The self consistent field and the structure of atoms. *Phys. Rev.* **32**, 339–348 (1928) <https://doi.org/10.1103/PhysRev.32.339>
- [45] Blinder, S.M.: Chapter 1 - introduction to the hartree-fock method. In: Blinder, S.M., House, J.E. (eds.) *Mathematical Physics in Theoretical Chemistry. Developments in Physical & Theoretical Chemistry*, pp. 1–30. Elsevier, Champaign, IL, USA (2019). <https://doi.org/10.1016/B978-0-12-813651-5.00001-2>
- [46] Yost, S.R., Head-Gordon, M.: Efficient implementation of NOCI-MP2 using the resolution of the identity approximation with application to charged dimers and long C-C bonds in ethane derivatives. *J. Chem. Theory Comput.* **14**(9), 4791–4805 (2018) <https://doi.org/10.1021/acs.jctc.8b00697>
- [47] Purvis, I. George D., Bartlett, R.J.: A full coupled-cluster singles and doubles model: The inclusion of disconnected triples. *J. Chem. Phys.* **76**(4), 1910–1918 (1982) <https://doi.org/10.1063/1.443164>
- [48] Vinod, V., Zaspel, P.: Assessing non-nested configurations of multifidelity machine learning for quantum-chemical properties. *Mach. Learn.: Sci. Technol.* **5**(4), 045005 (2024) <https://doi.org/10.1088/2632-2153/ad7f25>
- [49] Vinod, V., Zaspel, P.: Investigating data hierarchies in multifidelity machine learning for excitation energies. *J. Chem. Theory Comput.* **21**(6), 3077–3091 (2025) <https://doi.org/10.1021/acs.jctc.4c01491>
- [50] Bartók, A.P., Kondor, R., Csányi, G.: On representing chemical environments. *Phys. Rev. B* **87**(18), 184115 (2013) <https://doi.org/10.1103/PhysRevB.87.184115>
- [51] Schütt, K.T., Glawe, H., Brockherde, F., Sanna, A., Müller, K.-R., Gross, E.K.: How to represent crystal structures for machine learning: Towards fast prediction

- of electronic properties. *Phys. Rev. B* **89**(20), 205118 (2014) <https://doi.org/10.1103/PhysRevB.89.205118>
- [52] Behler, J.: Atom-centered symmetry functions for constructing high-dimensional neural network potentials. *J. Chem. Phys.* **134**(7), 074106 (2011) <https://doi.org/10.1063/1.3553717>
- [53] Gastegger, M., Schwiedrzik, L., Bittermann, M., Berzsenyi, F., Marquetand, P.: wACSF—weighted atom-centered symmetry functions as descriptors in machine learning potentials. *J. Chem. Phys.* **148**(24), 241709 (2018) <https://doi.org/10.1063/1.5019667>
- [54] Christensen, A.S., Bratholm, L.A., Faber, F.A., Lilienfeld, O.A.: FCHL revisited: Faster and more accurate quantum machine learning. *J. Chem. Phys.* **152**(4), 044107 (2020) <https://doi.org/10.1063/1.5126701>
- [55] Krämer, M., Dohmen, P.M., Xie, W., Holub, D., Christensen, A.S., Elstner, M.: Charge and exciton transfer simulations using machine-learned hamiltonians. *J. Chem. Theory Comput.* **16**, 4061–4070 (2020) <https://doi.org/10.1021/acs.jctc.0c00246>
- [56] Zaspel, P., Huang, B., Harbrecht, H., Von Lilienfeld, O.A.: Boosting quantum machine learning models with a multilevel combination technique: Pople Diagrams revisited. *J. Chem. Theory Comput.* **15**(3), 1546–1559 (2019) <https://doi.org/10.1021/acs.jctc.8b00832>
- [57] Vinod, V., Kleinekathöfer, U., Zaspel, P.: Optimized multifidelity machine learning for quantum chemistry. *Mach. Learn.: Sci. Technol.* **5**(1), 015054 (2024) <https://doi.org/10.1088/2632-2153/ad2cef>